Materials Today Bio 28 (2024) 101250

Contents lists available at ScienceDirect

Materials Today Bio

journal homepage: www.journals.elsevier.com/materials-today-bio

An injectable decellularized extracellular matrix hydrogel with cortical neuron-derived exosomes enhances tissue repair following traumatic spinal cord injury

Gang Wang [a,b,c,1], Qian Li [a,b,c,d,1], Sumei Liu [a,b,c], Mo Li [a,b,c], Baoguo Liu [a,b,c], Tianyao Zhao [a,b,c], Bochao Liu [a,b,c,**], Zhiguo Chen [a,b,c,*]

[a] Cell Therapy Center, Beijing Municipal Geriatric Medical Research Center, Xuanwu Hospital, Capital Medical University, National Clinical Research Center for Geriatric Diseases, and Key Laboratory of Neurodegenerative Diseases, Ministry of Education, Beijing, 100053, China
[b] Center of Neural Injury and Repair, Beijing Institute for Brain Disorders, Beijing, 100069, China
[c] Center of Parkinson's Disease, Beijing Institute for Brain Disorders, Beijing, 100069, China
[d] Department of Neurosurgery, Xuanwu Hospital, Capital Medical University, Beijing, 100053, China

ARTICLE INFO

Keywords:
Spinal cord injury
Cortical neurons
Exosomes
Umbilical cord mesenchymal stem cells
Decellularized extracellular matrix
Nerve regeneration

ABSTRACT

Traumatic spinal cord injury (SCI), known for its limited intrinsic regeneration capacity, often results in considerable neurological impairment. Studies suggest that therapeutic techniques utilizing exosomes (Exo) to promote tissue regeneration and modulate immune responses are promising for SCI treatment. However, combining exosome therapy with biomaterials for SCI treatment is not very effective. This study developed an adhesive hydrogel using exosomes secreted by cortical neurons derived from human induced pluripotent stem cells (iPSCs) and decellularized extracellular matrix (dECM) from human umbilical cord mesenchymal stem cells (hUCMSCs) to enhance motor function recovery post-SCI. In vitro assessments demonstrated the excellent cytocompatibility of the dECM hydrogel. Additionally, the Exo-dECM hydrogel facilitated the polarization of early M2 macrophages, reduced neuronal apoptosis, and established a pro-regenerative microenvironment in a rodent SCI model. Subsequent analyses revealed significant activation of endogenous neural stem cells and promotion of axon regeneration and remyelination at eight weeks post-surgery. The Exo-dECM hydrogel also promoted the functional recovery and preservation of urinary tissue in SCI-afflicted rats. These findings highlighted that the Exo-dECM hydrogel is a promising therapeutic strategy for treating SCI.

1. Introduction

Traumatic spinal cord injury (SCI) is defined by its limited inherent ability to regenerate, leading to significant neurological impairment. The pathological progression of SCI involves primary injury and secondary injury. Primary injury results from initial mechanical trauma and is marked by neuronal cell death, vascular damage, and disruption of the blood-spinal cord barrier. Secondary injury is triggered by hypoxia and subsequent biochemical changes. This phase is characterized by an inflammatory response, immune reactions, apoptosis, and demyelination at the site of injury [1–3]. These processes disrupt the local microenvironment, intensifying inflammation and neuronal damage. Consequently, strategies aimed at mitigating inflammation and enhancing neuronal survival are promising approaches for treating SCI.

Exosomes play a crucial role in cellular communication by transporting proteins, cytokines, mRNAs, and microRNAs [4,5]. Recently, exosomes released by various cell types have attracted considerable interest for enhancing the local microenvironment in SCI therapy [6,7].

* Corresponding author. Cell Therapy Center, Beijing Municipal Geriatric Medical Research Center, Xuanwu Hospital, Capital Medical University, National Clinical Research Center for Geriatric Diseases, and Key Laboratory of Neurodegenerative Diseases, Ministry of Education, Beijing, 100053, China.
** Corresponding author. Center of Parkinson's Disease, Beijing Institute for Brain Disorders, Beijing, 100069, China.
E-mail addresses: wanggang.neurobio@gmail.com (G. Wang), liqian0352@126.com (Q. Li), lsm-2007@163.com (S. Liu), limo110@163.com (M. Li), baoguo8325@163.com (B. Liu), neo_zty@163.com (T. Zhao), bochaoliu@xwhosp.org (B. Liu), chenzhiguo@gmail.com (Z. Chen).
[1] These authors have contributed equally to this work.

https://doi.org/10.1016/j.mtbio.2024.101250
Received 11 April 2024; Received in revised form 11 July 2024; Accepted 13 September 2024
Available online 14 September 2024

Advances in exosome-based treatments for SCI have improved patient outcomes [8]. Studies have highlighted the strong anti-inflammatory effects of exosomes on SCI, involving the reduction of key inflammatory markers, such as IL-1β, IL-6, TNF-α, interferon-γ, and granulocyte colony-stimulating factor [9,10]. Studies using a rat SCI model have shown that exosomes can promote M2 macrophage polarization, thereby reducing neuronal apoptosis, degeneration, and SCI-induced inflammatory responses [11,12]. Moreover, exosome administration enhances functional recovery by suppressing M1 microglial activation, alleviating neuroinflammation, and inhibiting A1 astrocyte activation [13]. These findings highlight the promising functions of exosomes as cell-free therapeutic agents for SCI treatment. However, their short half-life and rapid clearance by the immune system present challenges that limit their application. Therefore, developing a robust delivery strategy to ensure exosome retention and sustained release within injured spinal cord tissue is essential.

Natural hydrogels such as collagen, fibronectin, chitosan, hyaluronic acid, gelatin, alginate, and extracellular matrix (ECM) are widely recognized for their three-dimensional structure, injectability, biodegradability, and excellent compatibility with cells, making them extensively used in drug and cell delivery for regenerative medicine [14–16]. Recently, researchers have focused on decellularized extracellular matrix (dECM), which preserves natural ECM components and shows promise in tissue regeneration [17,18]. Studies have shown that dECM promotes the proliferation and differentiation of retinal progenitor cells into retinal neurons *in vivo*, highlighting its exceptional cytocompatibility [19]. Additionally, applying dECM hydrogels after spinal cord contusion was found to improve motor function recovery in rats [20]. Furthermore, dECM hydrogels have been investigated not only as a sustained-release platform for factors secreted by human adipose tissue-derived stromal cells but also as a delivery system for mesenchymal stem cells, creating a supportive microenvironment for nerve repair and showing promise in treating neurogenic disorders and injuries [21,22]. However, further assessment is needed to fully understand the potential of dECM hydrogels as exosome delivery vehicles for SCI treatment.

An injectable adhesive dECM hydrogel was developed in this study for the stable delivery of cortical neuron exosomes to treat SCI. The dECM hydrogel exhibited robust mechanical stability and excellent cytocompatibility, allowing effective injection into the injury site to fill the lesion cavity. Following implantation of the Exo-dECM hydrogel, significant polarization of M2 macrophages and activation of endogenous neural stem cells were observed. Moreover, axon regeneration and remyelination were facilitated at eight weeks post-implantation. Additionally, the enhanced polarization of M2 macrophages, activation of endogenous neural stem cells, regeneration of axons, and remyelination collectively contributed to improvements in functional recovery in a rat SCI model. This study revealed a promising therapeutic approach for SCI treatment using cortical neuron-derived exosomes delivered via a localized adhesive Exo-dECM hydrogel system.

2. Materials and methods

2.1. Cell culture and differentiation

Human induced pluripotent stem cells (hiPSCs) were differentiated into cortical neurons using a previously established method [23]. Initially, hiPSCs were plated on Matrigel-coated culture dishes in TeSR™-E8™ medium (STEMCELL, Cat# 05990) supplemented with the 10 mM ROCK inhibitor Y-27632 (YESEN, Cat# 52604ES25) on day −2. On day 0 of differentiation, the medium was changed to include 1 μM dorsomorphin (APExBIO, Cat# B3252). The differentiation medium consisted of DMEM/F12 (Gibco, Cat# 11320033) supplemented with 2 % B27 (Gibco, Cat# 17504044), 1 % GlutaMAX™ (Gibco, Cat# 35050061), 1 % N2 (Gibco, Cat# 17502048), 1 % nonessential amino acids (Gibco, Cat# 11140050), 1 mM sodium pyruvate (Gibco, Cat# 11360070), 1 % BSA (Amresco, Cat# 0332-100G), 100 U/mL penicillin−streptomycin (Gibco, Cat# 15140122), 5 μg/mL insulin (Roche, Cat# 11376497001), and 0.1 mM 2-mercaptoethanol (Gibco, Cat# 21985023). The medium was replaced every 48 h. From day 16 onward, the medium was replaced every 48 h with fresh differentiation medium. On day 30, Neurobasal™-A medium (Gibco, Cat# 10888022) supplemented with 2 % B27 and 1 % GlutaMAX™ was used to replace half of the medium, with subsequent changes every five days until day 70 of differentiation.

2.2. Exosome isolation and identification

Exosomes were extracted from neuron-conditioned medium using established techniques [24]. Initially, culture supernatants from iPSC-neurons were subjected to sequential centrifugation at 300×*g* for 10 min and 2000×*g* for 10 min at 4 °C to eliminate cells and debris. The samples were then concentrated to 200 μL using an Amicon Ultra15 Centrifuge Filter Unit (Millipore, Cat# UFC910096). The concentrated solutions were thoroughly mixed with Total Exosome Isolation Reagent (Invitrogen, Cat# 4478359) and incubated overnight at 4 °C. The following day, the mixture was centrifuged at 10,000×*g* for 1 h at 4 °C. The resultant exosomes were resuspended in Phosphate-buffered saline (PBS, pH 7.4) and subjected to ultracentrifugation at 100,000×*g* for 70 min at 4 °C. Subsequently, the exosome pellet was resuspended in PBS and centrifuged again at 100,000×*g* for 70 min at 4 °C for further purification. The purified exosomes were collected, filtered through a 0.22-μm pore filter (Millipore, Cat# SLGPR33RB), and either used for subsequent experiments or stored at −80 °C.

Exosome morphology was analyzed by transmission electron microscopy (Hitachi). Nanoparticle tracking analysis (NTA) with a particle size analyzer (Particle Metrix) was used to determine the particle concentration and size distribution. Furthermore, Western blotting was performed to assess the presence of specific marker proteins in the exosomes, such as CD81 (Abcam, Cat# ab109201), HSP70 (Abcam, Cat# ab181606), and Tsg101 (Abcam, Cat# ab125011).

2.3. Quantification and labeling of cortical neuron-derived exosomes

The protein content of the exosomes was quantified using a Pierce Micro BCA Protein Assay Kit (Invitrogen, Cat# 23235). For fluorescent labeling, the exosomes were resuspended in PBS and treated with 2 mg/mL DiI stain (Invitrogen, Cat# D3911) at a ratio of 1:100, followed by incubation for 30 min at 37 °C. Any excess DiI stain was then removed using an Amicon Ultra15 Centrifuge Filter Unit at 4000×*g* for 20 min at 4 °C.

2.4. Western blotting

The exosomes were treated with RIPA lysis buffer (Cell Signaling Technology, Cat# 9806S) containing a protease inhibitor cocktail (Roche, Cat# 4693159001). Protein concentrations were determined using a BCA Protein Assay Kit (CWBIO, Cat# CW0014S). SDS-PAGE with MOPS running buffer was used to separate the proteins, which were then transferred onto PVDF membranes (Millipore, Cat# IPVH00005) and blocked in TBS-T (137 mM sodium chloride, 20 mM Tris, and 0.1 % Tween-20 at pH 7.6) with 5 % skim milk for 1 h at room temperature. The Exosome Panel (Abcam, Cat# ab275018), which included antibodies against CD81, HSP70, and TSG101, was incubated with the membranes overnight at 4 °C at a 1:1000 dilution. After washing three times with TBS-T, the membranes were exposed to HRP-conjugated secondary antibody (Servicebio, Cat# GB23303 for goat anti-rabbit) for 2 h at room temperature. Immunoreactive bands were visualized using an enhanced chemiluminescence system (Biosharp, Cat# BL520), and images were captured using a ChemiDoc Touch Imaging System (Servicebio, Cat# SCG-W3000).

2.5. Preparation of the hUCMSC-dECM

Human umbilical cord mesenchymal stem cells (hUCMSCs) at passage 3 were harvested following established procedures [25]. Initially, hUCMSCs were seeded onto 10 cm culture dishes at a density of 10,000 cells/cm^2. When the cells reached at least 90 % confluence, a maintenance medium containing 50 μg/mL L-ascorbic acid (Sigma–Aldrich, Cat# A4544-100G) and 15 % Fetal Bovine Serum (Gibco, Cat# 10270106) was used to induce extracellular matrix (ECM) secretion. The medium was replaced every two days for seven days. For decellularization, the cells were washed three times with PBS, followed by treatment with ultrapure water at 37 °C for 10 min. After removing the ultrapure water, the samples were exposed to a solution of 3 % Triton X-100 and 2 % sodium dodecyl sulfate (Sigma–Aldrich, Cat# 436143-25G) at 37 °C for 5 min. After three PBS washes, the resulting dECM derived from the hUCMSCs was stored in PBS supplemented with 1 % antibiotic-antimycotic solution (Gibco, Cat# 15240062) at 4 °C for up to two weeks.

2.6. Neural precursor cell culture

Neural precursor cells (NPCs) were seeded onto Matrigel-coated 24-well plates (Corning, Cat# 354277) with dECM at a density of 10,000 cells/cm^2. The adhesion of NPCs was assessed at 12 h, 24 h, and 48 h post-seeding using fluorescence microscopy with GFP staining (GenScript, 1:400 dilution, Cat# A01388). To measure NPC proliferation, an EdU incorporation assay was performed with BeyoClick™ EdU-555 (Beyotime, Cat# C0075S) following the manufacturer's protocol. Initially, NPCs were cultured in Matrigel and dECM-coated 24-well plates for 24 h. The following day, half of the culture medium was replaced with fresh medium containing 10 μM EdU. After 24 h, the cells were fixed with 4 % paraformaldehyde for 15 min at room temperature, washed with PBS and 0.3 % Triton X-100 PBS, and then treated with click reaction buffer (in the dark) for 30 min. The nuclei were counterstained with 10 μg/mL DAPI (YEASEN, Cat# 40727ES10), and images were captured using a confocal microscope (Leica, TCS SP5).

2.7. Cell apoptosis assay

Apoptotic cells in the spinal cord lesion site were identified using a TUNEL Apoptosis Assay Kit (Beyotime, Cat# C1086) according to the manufacturer's instructions. In brief, the sections were incubated in TUNEL detection solution (Cy3-dUTP labeling solution:TdT enzyme = 9:1) for 60 min at 37 °C in the dark. Nuclei were counterstained with DAPI, and imaging was performed using a confocal microscope.

2.8. Animals and ethics statement

Healthy adult female Sprague–Dawley rats (200–220 g), known for being more docile and having reduced susceptibility to urinary tract infections post-injury compared to male rats, were selected for this study. The female rats were purchased from Vital River Laboratories (Beijing, China) and housed in a specific pathogen-free (SPF) environment with ad libitum access to food and water. All animal procedures adhered to the guidelines outlined in the Chinese Ministry of Public Health Guide and the US National Institutes of Health Guide for the Care and Use of Laboratory Animals. The study protocol was approved by the Animal Ethics Committee of Xuanwu Hospital Capital Medical University (Approval number: XW-20210423–2).

2.9. Spinal cord contusion model establishment and treatment

Healthy adult female Sprague–Dawley rats were randomly assigned to five groups: the sham group (n = 8), the PBS group (n = 8), the Exo group (n = 8), the dECM group (n = 8), and the Exo-dECM group (n = 8). Rats were anesthetized using a compound anesthetic administered intraperitoneally. A spinal cord contusion model was induced by carefully exposing and contusing the T9 – T10 segment of the spinal cord (velocity: 1.5 m/s, depth: 1.7 mm, duration: 85 ms). Different treatment strategies were applied at the spinal cord lesion site. In the SCI group, PBS was injected to control for the potential effects of the injection procedure. Bladder emptying was performed twice daily for two weeks post-SCI in each rat. Behavioral, morphological, and histological assessments were conducted within eight weeks post-operation.

2.10. Immunohistochemical staining

Cultured cells or frozen tissue slices were blocked with 5 % donkey serum (Jackson, Cat# 017-000-121) for 1 h at 37 °C. Primary antibodies were applied at 4 °C overnight as follows: mouse anti-OCT3/4 antibody (Abcam, 1:400 dilution, Cat# 200834), rabbit anti-Ki-67 antibody (Sigma-Aldrich, 1:400 dilution, Cat# Ab9260), rabbit anti-TBR1 antibody (Abcam, 1:400 dilution, Cat# ab31940), rat anti-CTIP2 antibody (Abcam, 1:400 dilution, Cat# ab18465), rabbit anti-FOXP2 antibody (Abcam, 1:5000 dilution, Cat# ab16046), rabbit anti-SATB2 antibody (Abcam, 1:1000 dilution, Cat# ab34735), mouse anti-MAP2 antibody (Abcam, 1:300 dilution, Cat# ab32454), mouse anti-NeuN antibody (Abcam, 1:500 dilution, Cat# 104224), mouse anti-NF200 antibody (Millipore, 1:800 dilution, Cat# MAB5262), mouse anti-Tuj1 antibody (Santa Cruz, 1:400 dilution, Cat# sc-51670), mouse anti-CD68 antibody (Abcam, 1:400 dilution, Cat# ab955), and mouse anti-CD206 antibody (Abcam, 1:1000 dilution, Cat# ab8918), mouse anti-Nestin antibody (Millipore, 1:200 dilution, Cat# MAB353), rabbit anti-GFAP antibody (ZSGB-BIO, 1:400 dilution, Cat# ZA-0529), and rat anti-MBP antibody (Proteintech, 1:200 dilution, Cat# 10458-1-AP). Subsequently, the following secondary antibodies were used: FITC AffiniPure Donkey Anti-Mouse IgG (H + L) (Jackson, 1:200 dilution, Cat# 715-095-151), Cy™3 AffiniPure Donkey Anti-Rabbit IgG (H + L) (Jackson, 1:400 dilution, Cat# 711-165-152), Cy™5 AffiniPure Donkey Anti-Mouse IgG (H + L) (Jackson, 1:200 dilution, Cat# 715-175-151), and Cy™5 AffiniPure Donkey Anti-Rat IgG (H + L) (Jackson, 1:200 dilution, Cat# 712-175-150). The samples were incubated with corresponding secondary antibodies for 2 h at room temperature. Nuclei were counterstained with DAPI. Imaging was conducted using a confocal microscope (Leica), and the ImageJ software was used to quantify the number/area of positive cells.

2.11. Electrophysiology

MEP measurements were conducted on different groups eight weeks post-operation, following methods described in another study [26]. Rats were deeply anesthetized using a compound anesthetic. Electrical stimulation (5 mA, 0.1 ms, 1 Hz) was applied to the cerebral motor cortex. MEPs were recorded from the gastrocnemius muscle, with the ground electrode placed subcutaneously. The amplitude of MEPs was quantified using a Keypoint-II bichannel evoked potentials/electromyograph system (Dantec Dynamics).

2.12. Functional behavior assessment

The functional recovery of the rats was evaluated using the Basso, Beattie, and Bresnahan (BBB) locomotor rating scale, inclined plane test, and footprint analysis. In the BBB test, rats were placed in an open field and observed weekly for 5 min post-surgery to assess their motion characteristics. For the inclined plane test, rats were positioned on an angle-adjustable board, and the maximum angle they could maintain for 5 s without falling was recorded eight weeks after surgery. Footprint analysis involved dipping the hind paws of the rats in blue dye and allowing them to walk across a dark passage covered with white paper [27]. Footprints were scanned and analyzed for stride length using the ImageJ software. Two independent observers who were blinded to the treatments conducted all the assessments.

2.13. Histological analysis

The histological analysis included hematoxylin and eosin (H&E) staining (Beyotime, Cat# C0105S), Masson's trichrome staining (Beyotime, Cat# C0189S), and Luxol fast blue (LFB) staining (Solarbio, Cat# G3242). The morphology of the spinal cord and bladder was evaluated using H&E staining according to the manufacturer's protocols. Masson's trichrome staining was performed to assess bladder tissue fibrosis following the manufacturer's instructions. LFB staining was performed to detect myelin sheaths in regenerated nervous tissue following the manufacturer's guidelines. Imaging was performed using a Nikon microscope, and quantification analysis was performed using the ImageJ software.

2.14. Statistical analysis

The data are expressed as the mean ± standard deviation (SD). Student's *t*-test was used to compare two groups using the Stata 7.0 software package. For multiple comparisons, one-way analysis of variance (ANOVA) was performed using GraphPad Prism 7.0 software. Statistical significance was set at $p < 0.05$, with 'ns' indicating no significant difference.

3. Results

3.1. Characterization of cortical neuron-derived exosomes differentiated from hiPSCs

Human induced pluripotent stem cells (iPSCs) were differentiated into cortical neurons using a previously published protocol [23]. The induced cells exhibited typical neuronal morphological characteristics and expressed neuron-specific class III beta-tubulin (Tuj1) at 55 days of differentiation (Figs. S1B and 1B). Markers associated with cortical neurons were assessed to confirm the identity of the differentiated neurons. Robust expression of cortical neuron-specific markers, including TBR1, CTIP2, FOXP2, and SATB2, was observed (Fig. 1B). Furthermore, after 70 days of differentiation, the neurons expressed markers specific to mature neurons (MAP2, NF200, and NeuN) (Fig. 1C and D), indicating successful differentiation of the hiPSCs into cortical neurons and subsequent maturation into functional neurons. Subsequently, conditioned medium from the cortical neurons was harvested, and exosomes were isolated following established procedures. Transmission electron microscopy revealed the round vesicle-shaped morphology of the exosomes derived from cortical neurons (Fig. 1E). Nanoparticle tracking analysis revealed that the average diameter of cortical neuron-derived exosomes was approximately 136.0 nm, with an average concentration of 9.5×10^{10}/mL (Fig. 1F). Western blotting analysis confirmed the presence of CD81, HSP70, and TSG101 in the exosomes, while calnexin was not detected (Fig. 1G). Together, these results indicated that cortical neuron-derived exosomes were successfully obtained.

3.2. Characterization and cytocompatibility of hUCMSC-derived dECM

Human umbilical cord mesenchymal stem cells (hUCMSCs) at passage 3 were cultured for seven days with 50 μg/mL L-ascorbic acid and subsequently decellularized following a well-established protocol [28]. Before decellularization, the hUCMSCs were found to be densely packed under a light microscope (Fig. 2A). Post-decellularization, evaluations were conducted, including DAPI staining, H&E staining, and quantification of residual DNA content, to assess the effectiveness of the decellularization process. DAPI and H&E staining indicated minimal residual nuclei within the decellularized extracellular matrix (dECM) (Figs. S2A and C). Furthermore, DNA quantification demonstrated a significant decrease in DNA content in the dECM compared to that in the original hUCMSCs (Fig. S2B). These findings collectively confirmed the successful removal of cellular components from hUCMSCs through decellularization. Scanning electron microscopy was performed to investigate the micromorphology of the dECM, revealing a complex 3D network structure consisting of filamentous structures and granular particles (Fig. 2B).

To assess the cytocompatibility of the dECM *in vitro*, neural precursor cells (NPCs) were cultured on dECM, tissue culture plastic (TCP), or Matrigel as a control (Fig. 2C). Subsequent evaluation of NPC adhesion and proliferation on these substrates involved immunofluorescence staining and an EdU assay. Immunofluorescence analysis revealed robust NPC growth on both dECM and Matrigel, whereas growth was limited on TCP (Fig. 2D). A significant difference was observed in the number of cells among the dECM, TCP, and Matrigel groups (Fig. 2E–G), which might be contributed to the intricate 3D network structure of dECM. Furthermore, NPC proliferation significantly increased when the cells were cultured on dECM (Fig. 2H, I and Figs. S3A and B), potentially attributed to the roles of granular particles observed in Fig. 2B. These results indicated that the dECM exhibits favorable cytocompatibility, suggesting its potential to support NPC growth and proliferation *in vitro*.

3.3. Characterization of the Exo-dECM hydrogel

To confirm how exosomes are distributed within the dECM hydrogel, they were first labeled with DiI and then encapsulated in the dECM hydrogel *in vitro*. Three-dimensional immunofluorescence images obtained by scanning through z-stacks revealed a consistent and widespread distribution of exosomes throughout the dECM hydrogels (Fig. S2E). Subsequent long-term release experiments revealed an initial burst release of approximately 60 % of the exosomes from the dECM hydrogel within the first week, followed by a continuous release exceeding 80 % over the next 28 days (Fig. S2D). This gradual and steady release of exosomes from dECM hydrogels indicated that they can effectively repair SCI.

3.4. Exo-dECM hydrogels attenuate the short-term inflammatory response following SCI

The inflammatory response is crucial for reactions to central nervous system injuries [29]. To investigate the effect of the Exo-dECM hydrogel on this response, proinflammatory (M1) and anti-inflammatory (M2) macrophages were evaluated through immunofluorescence staining. Two weeks after surgery, a greater number of CD68-positive macrophages were observed at the spinal cord lesion site. A significant difference in the number of CD68-positive macrophages was detected between the Exo-dECM hydrogel-treated group and the SCI group (Fig. 3B and C). Furthermore, the presence of M2 macrophages at the lesion site was confirmed by assessing the expression of CD206, a marker specific to M2 macrophages. Treatment with the Exo-dECM hydrogel led to greater accumulation of CD206-positive cells (Fig. 3B and D).

Given that neuronal apoptosis, which is triggered by the inflammatory microenvironment, is a defining characteristic of early-stage SCI [30], we investigated the protective effects of the Exo-dECM hydrogel against neuronal apoptosis by conducting a TUNEL assay. The number of TUNEL-positive neuronal cells was significantly lower in the Exo-dECM hydrogel group than in the other experimental groups (Fig. 3E and F). These findings suggested that the Exo-dECM hydrogel may not only stimulate the polarization of M2 macrophages but also enhance the short-term survival of neuronal cells following SCI.

3.5. Exo-dECM hydrogels enhance functional recovery and reduce cavity formation following SCI

To assess functional recovery after SCI, we conducted several tests, including the BBB open-field locomotor rating scale, inclined plane test, and footprint analysis, at eight weeks post-operation. The BBB scores showed a gradual improvement in locomotor function in the SCI groups,

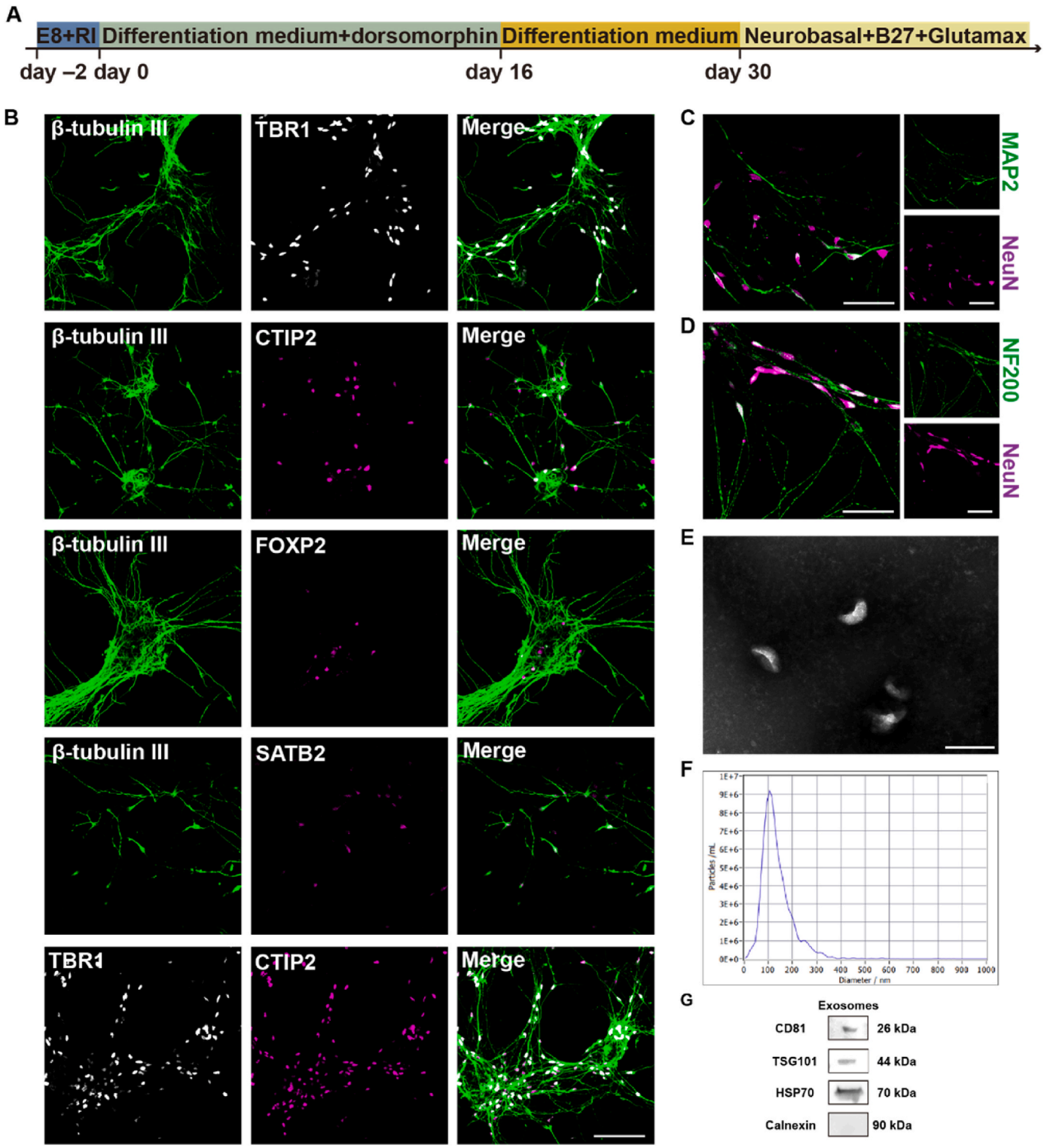

Fig. 1. Differentiation of hiPSCs into cortical neurons and characterization of exosomes derived from cortical neurons. (A) The process of hiPSC differentiation into cortical neurons is schematically represented. (B) Immunofluorescence images showing the expression of β-tubulin III, TBR1, CTIP2, FOXP2, and SATB2 in hiPSC-derived cortical neurons at 55 days of differentiation; scale bar: 100 μm. (C) Immunofluorescence images showing MAP2 and NeuN expression in hiPSC-derived cortical neurons after 70 days of differentiation; scale bar: 100 μm. (D) Immunofluorescence images demonstrating NF200 and NeuN expression in hiPSC-derived cortical neurons after 70 days of differentiation; scale bar: 100 μm. (E) Transmission electron microscopy images showing the morphology of the exosomes; scale bar: 200 nm. (F) Nanoparticle tracking analysis data illustrating the particle size distribution of the exosomes. (G) Western blotting results indicate the presence of the exosomal surface markers CD81, TSG101, and HSP70.

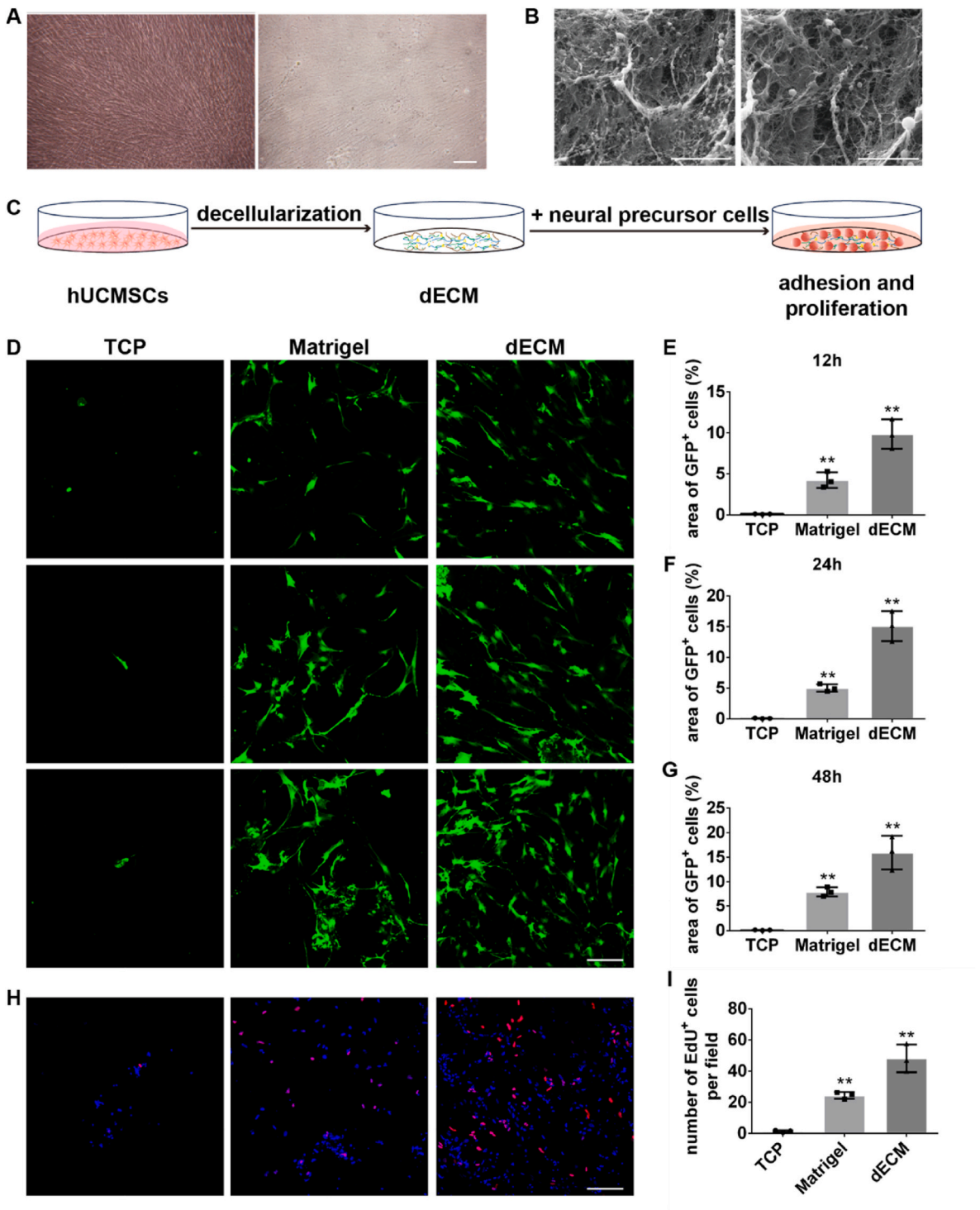

Fig. 2. Characterization and cytocompatibility of dECM. (A) Light microscopic characteristics of pre-decellularized hUCMSCs and post-decellularized dECM; scale bar: 100 μm. (B) Scanning electron micrographs illustrating the ultrastructure of the dECM and a local high-magnification image; scale bars: 10 μm and 5 μm. (C) Schematic representation of the experimental process of culturing neural precursor cells (NPCs) on dECM. (D) Representative immunofluorescence staining of GFP (green) in NPCs cultured on TCP, Matrigel, and dECM; scale bar: 100 μm. (E–G) Quantification of GFP-positive cells in different groups after 12 h, 24 h, and 48 h of culture. The graphs depict the mean ± SD (n = 3; $^{**}p < 0.01$ versus the TCP group). (H) Representative images of immunofluorescence staining for EdU (red) in NPCs cultured on TCP, Matrigel, and dECM. Nuclei were stained with DAPI; scale bar: 100 μm. (I) Quantification of EdU-positive cells in each group after 24 h of culture. The graphs show the mean ± SD (n = 3; $^{**}p < 0.01$ versus the TCP group).

and locomotor function plateaued by four weeks post-operation (Fig. 4A). Compared with those in the SCI group, the BBB scores in the Exo-dECM hydrogel treatment group were significantly greater, indicating enhanced recovery of locomotor function (Fig. 4A). Moreover, treatment with the Exo-dECM hydrogel improved the inclination angle compared to that of the other groups (Fig. 4C). According to the footprint analysis, the hind limb dragging observed in the SCI group indicated impaired locomotion, whereas clear footprints were visible in the treatment groups, emphasizing the functional benefits of Exo-dECM hydrogel treatment (Fig. 4E). Quantitative analysis also revealed a

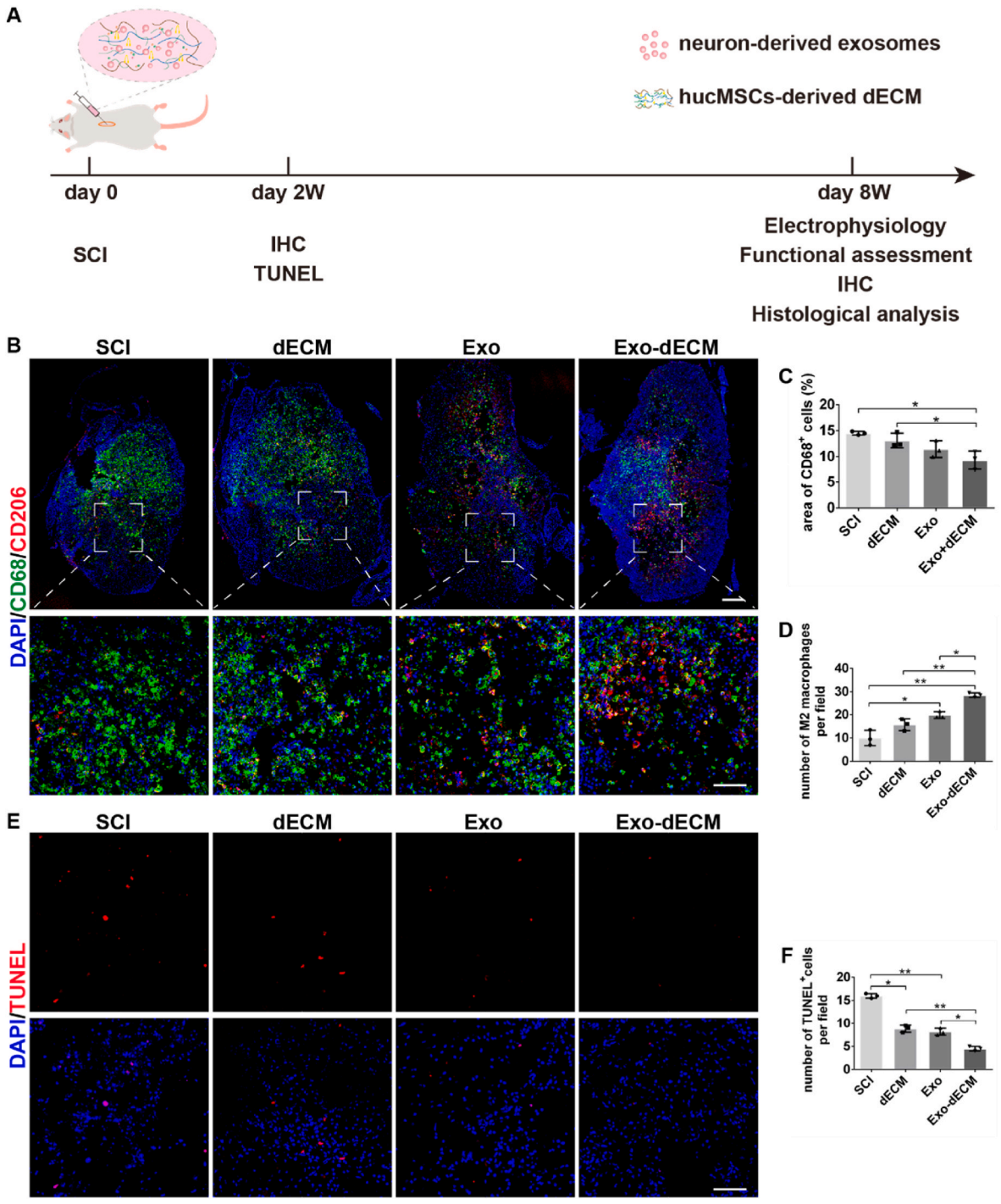

Fig. 3. The Exo-dECM hydrogel attenuates the short-term inflammatory response. (A) Schematic representation depicting the timeline of the *in vivo* experiments. (B) Representative immunofluorescence staining of CD206 (red) and CD68 (green) at the spinal cord lesion site two weeks post-operation. Nuclei were counterstained with DAPI; scale bars: 250 μm and 100 μm. (C–D) Quantification of macrophages ($CD68^+$) and M2 macrophages ($CD68^+$ and CD206+). The graphs display the mean ± SD (n = 3; $*p < 0.05$ and $**p < 0.01$). Each data point represents one rat. (E) Representative images of TUNEL staining at the spinal cord lesion site two weeks post-operation. Nuclei were stained with DAPI; scale bar: 100 μm. (F) Quantification of TUNEL-positive cells. The graphs show the mean ± SD (n = 3; $*p < 0.05$ and $**p < 0.01$). Each data point represents one rat.

significant increase in stride length in the Exo-dECM hydrogel group compared to the other groups, indicating improved gait dynamics and motor function (Fig. 4F).

In accordance with the observed improvements in behavioral assessments, electrophysiological evaluations performed at eight weeks post-surgery revealed a favorable trend toward enhanced motor recovery in animals treated with the Exo-dECM hydrogel (Fig. 4H and I). Furthermore, histological examinations using H&E staining and LFB staining revealed a significant reduction in cavity size, along with increased infiltration of nerve cells and improved fiber formation in the Exo-dECM hydrogel- and Exo-treated groups compared to the SCI group (Fig. 4J, K and Fig. S4). These results collectively suggested that Exo-dECM hydrogel treatment can promote functional recovery and reduce cavity formation following SCI.

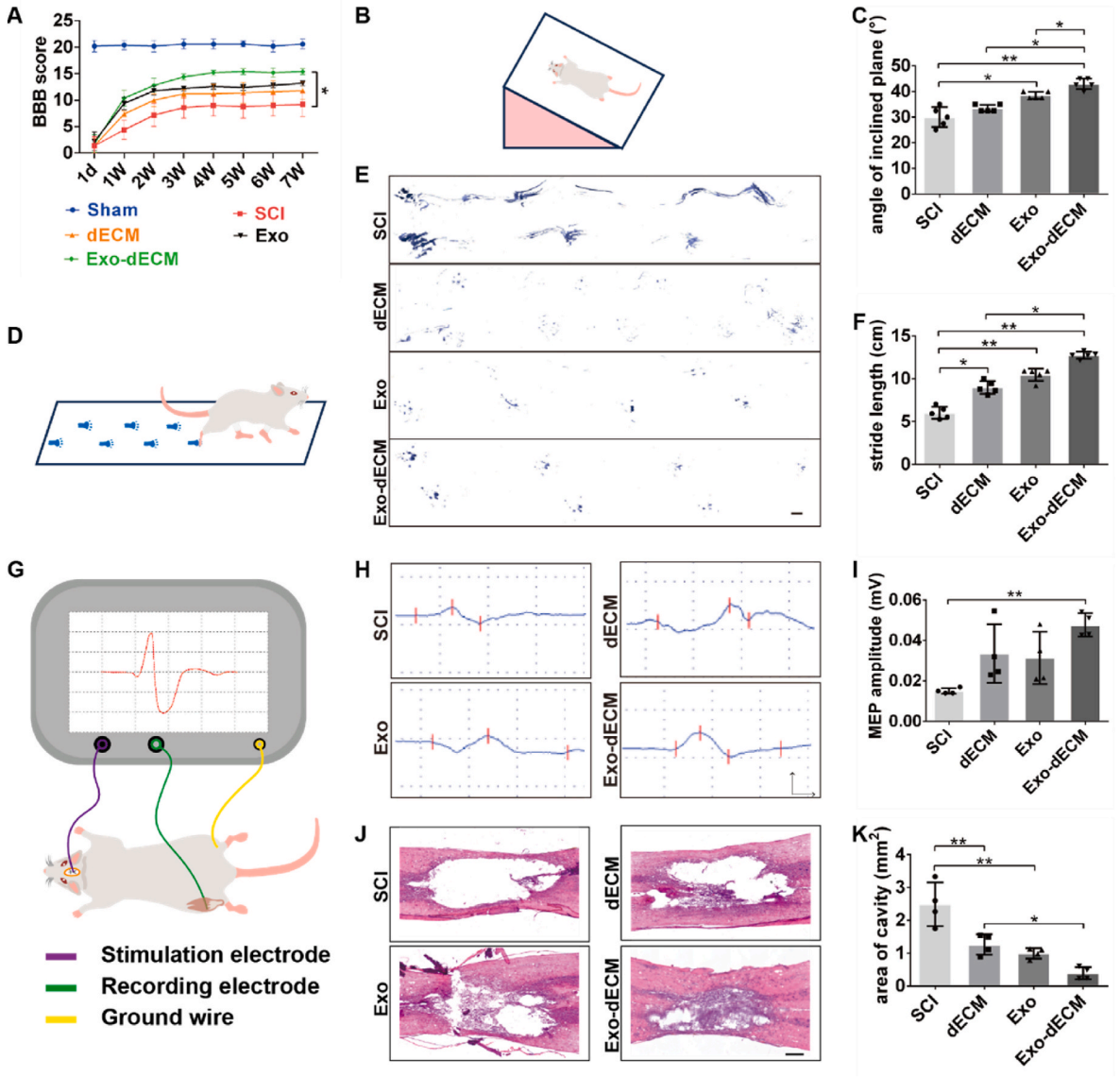

Fig. 4. Exo-dECM hydrogel improved functional recovery. (A) BBB score within eight weeks after surgery. *, SCI vs. Exo-dECM. The graphs show the mean ± SD (n = 4; $*p < 0.05$). (B) Schematic diagram of the inclined plane test. (C) Quantification of the maximum angle of the inclined plane. The graphs show the mean ± SD (n = 4; $*p < 0.05$ and $**p < 0.01$). Each dot represents a rat. (D) Schematic diagram of footprint analysis. (E) Representative images of footprint analysis in different groups at eight weeks after surgery; scale bar: 10 mm. (F) Quantification of hindlimb stride length. The graphs show the mean ± SD (n = 4; $*p < 0.05$ and $**p < 0.01$). Each dot represents a rat. (G) Schematic diagram of the electrophysiology experiment. (H) Representative images of the different groups subjected to electrophysiology at eight weeks after surgery; scale bar: 0.05 mV. (I) Quantification of the amplitude of motor-evoked potentials. The graphs show the mean ± SD (n = 4, $**p < 0.01$). Each dot represents a rat. (J) Representative H&E staining images at the lesion site of the spinal cord eight weeks after surgery; scale bar: 500 μm. (K) Quantification of the lesion cavity area. The graphs show the mean ± SD (n = 4; $*p < 0.05$ and $**p < 0.01$). Each dot represents a rat.

3.6. Exo-dECM hydrogel enhances NSC activation and may facilitate NSC differentiation into neuronal cells following SCI

Neural stem cells (NSCs) that were previously quiescent may become activated and migrate toward the injury site following SCI [31]. To assess NSC activation after Exo-dECM hydrogel treatment, the expression of Nestin, a marker of NSCs, in both the rostral and caudal regions surrounding the lesion site was analyzed through immunofluorescence staining. The results indicated a significant increase in the number of Nestin-positive cells in the Exo-dECM hydrogel group compared to that in the SCI group (Fig. 5A). Quantitative analysis further revealed a substantial increase in Nestin-positive cell counts in both the rostral and caudal regions following Exo-dECM hydrogel treatment (Fig. 5C and D). Moreover, NSC activation induced by Exo-dECM hydrogel treatment might enhance neuronal presence at the spinal cord lesion site. Subsequent evaluation of neurons using NeuN, a neuron-specific marker, revealed a significant increase in the number of neurons in the Exo-dECM hydrogel group compared to that in the SCI group (Fig. 5B). Quantitative assessment confirmed that the number of NeuN-positive neurons surviving in the Exo-dECM hydrogel group was more than double that in the SCI group (Fig. 5E and F). These findings suggest that Exo-dECM hydrogel treatment promotes NSC activation and may support the differentiation of NSCs into neuronal cells, thus promoting neural repair following SCI.

3.7. Exo-dECM hydrogel promotes endogenous neurogenesis and reduces astroglial scar formation following SCI

To further investigate how Exo-dECM hydrogels influence neuronal differentiation, this study examined endogenous neurogenesis and

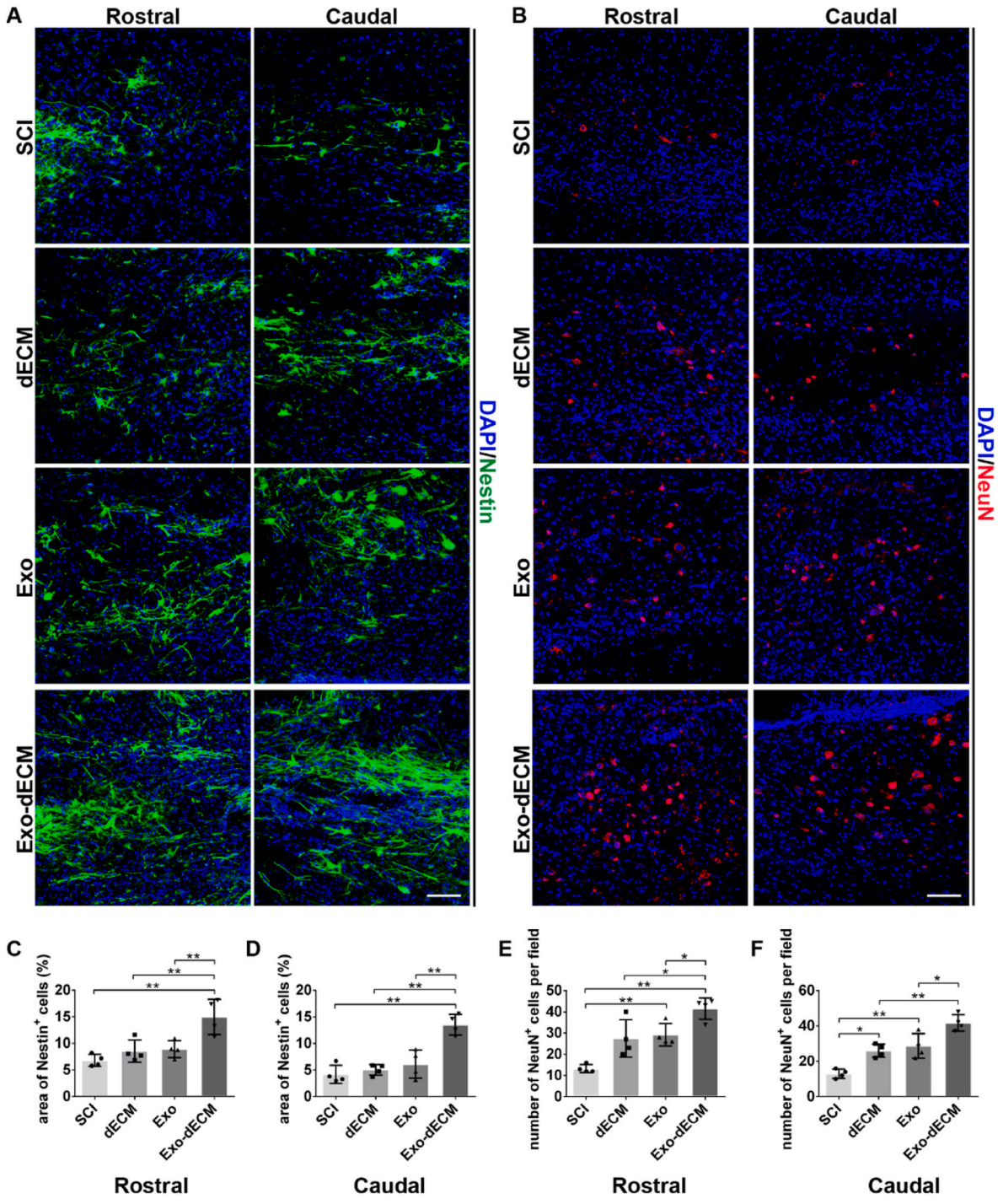

Fig. 5. Exo-dECM hydrogel enhances NSC activation and may facilitate NSC differentiation into neuronal cells. (A) Representative immunofluorescence staining of Nestin (green) rostral and caudal to the lesion site eight weeks after the operation. Nuclei were stained with DAPI; scale bar: 100 μm. (B) Representative immunofluorescence staining of NeuN (red) rostral and caudal to the lesion site eight weeks after the operation. Nuclei were stained with DAPI; scale bar: 100 μm. (C–D) Quantification of Nestin-positive cells rostral and caudal to the lesion site. The graphs show the mean ± SD (n = 4; $^{**}p < 0.01$). Each dot represents a rat. (E–F) Quantification of NeuN-positive cells rostral and caudal to the lesion site. The graphs show the mean ± SD (n = 4; $^{*}p < 0.05$ and $^{**}p < 0.01$). Each dot represents a rat.

astroglial scar formation at the spinal cord lesion site. Immunostaining of spinal cord tissue sections for Tuj1, a marker of immature neurons, revealed a greater abundance of Tuj1-positive cells originating from NSCs in the Exo-dECM hydrogel group than in the dECM hydrogel and SCI groups (Fig. 6A). Quantitative analysis confirmed a significant increase in the number of Tuj1-positive cells across the rostral, central, and caudal regions of the lesion site in the Exo-dECM hydrogel group (Fig. 6B–D). Additionally, excessive reactive astrocytes at the lesion site can hinder nerve fiber penetration and reconstruction. Quantitative assessment of GFAP-positive glial cells demonstrated a considerable reduction in glial cell numbers in the caudal region of the lesion site (Fig. 6G). These results indicated that treatment with the Exo-dECM hydrogel promoted endogenous neurogenesis and mitigated astroglial scar formation to a certain extent.

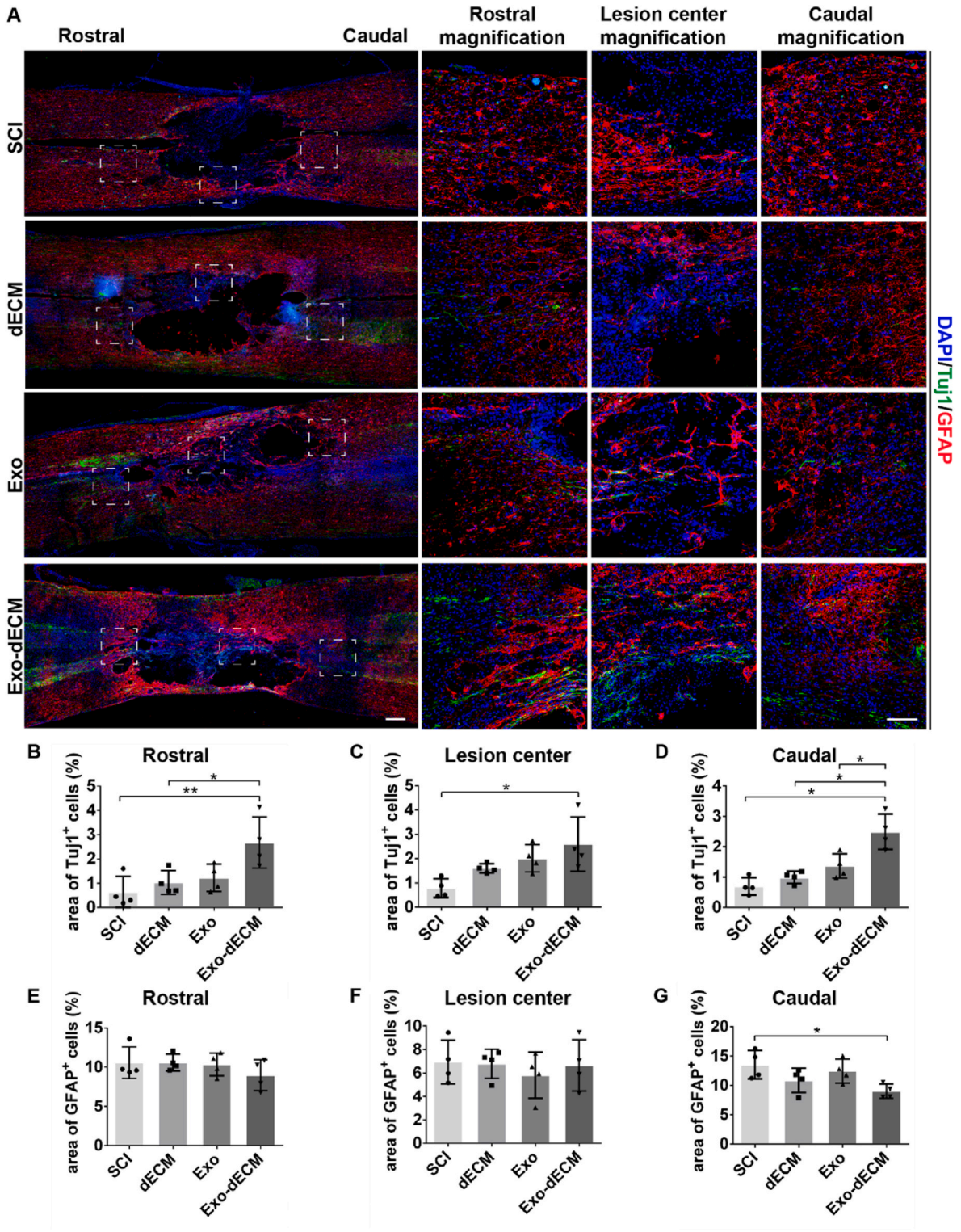

Fig. 6. Exo-dECM hydrogel promotes endogenous neurogenesis. (A) Representative immunofluorescence staining of β-tubulin III (Tuj1, green) and glial fibrillary acidic protein (GFAP, red) at the lesion site of the spinal cord eight weeks after the operation. Nuclei were stained with DAPI; scale bars: 250 μm and 100 μm. (B–D) Quantification of Tuj1-positive cells rostral, central, and caudal to the lesion site. The graphs show the mean ± SD (n = 4; $*p < 0.05$ and $**p < 0.01$). Each dot represents a rat. (E–F) Quantification of GFAP-positive cells rostral, central, and caudal to the lesion site. The graphs show the mean ± SD (n = 4; $*p < 0.05$). Each dot represents a rat.

3.8. Exo-dECM hydrogel promotes axon regeneration and remyelination following SCI

Given the limited regenerative capacity of the central nervous system (CNS), enhancing axonal regeneration is necessary for treating SCI. We investigated the expression of NF200, a marker of neurite outgrowth, in the injured spinal cord eight weeks after surgery to assess neurofilament extension. The SCI group exhibited minimal cavity repair with few NF-positive fibers (Fig. 7A). In contrast, treatment with the Exo-dECM hydrogel significantly increased the density and quantity of NF-

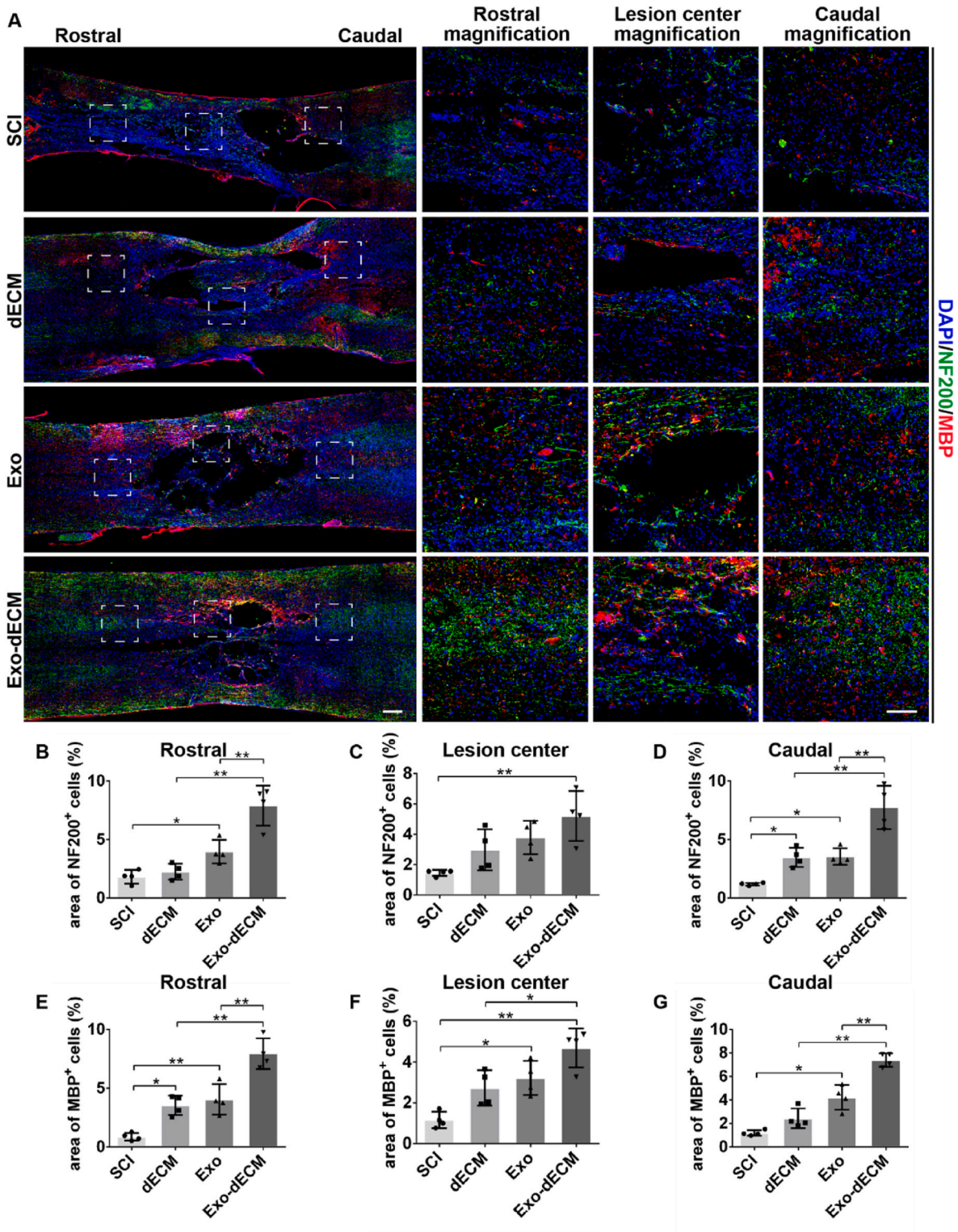

Fig. 7. Exo-dECM hydrogel promoted axon regeneration and remyelination. (A) Representative immunofluorescence staining of neurofilaments (NF200, green) and myelin basic protein (MBP, red) at the lesion site of the spinal cord eight weeks after surgery. Nuclei were stained with DAPI; scale bars: 250 μm and 100 μm. (B–D) Quantification of NF200-positive cells rostral, central, and caudal to the lesion site. The graphs show the mean ± SD (n = 4; $^{*}p < 0.05$ and $^{**}p < 0.01$). Each dot represents a rat. (E–G) Quantification of MBP-positive cells rostral, central, and caudal to the lesion site. The graphs show the mean ± SD (n = 4; $^{*}p < 0.05$ and $^{**}p < 0.01$). Each dot represents a rat.

positive fibers, highlighting its superior regenerative potential (Fig. 7A–D). Additionally, remyelination, which is essential for axon regeneration, was assessed by examining the expression of myelin basic protein (MBP), a marker of the myelin sheath, through immunofluorescence staining across different groups eight weeks after surgery. Both the Exo and dECM groups exhibited greater MBP expression than did the SCI group, with the Exo-dECM group showing the most significant improvement (Fig. 7E–G). These findings confirmed that Exo-

dECM treatment effectively promoted the formation of myelinated nerve fibers, thus enhancing neural repair mechanisms in SCI.

3.9. Exo-dECM hydrogel treatment attenuates pathological damage and ameliorates bladder dysfunction following SCI

Bladder dysfunction commonly accompanies SCI and serves as an indirect indicator of recovery. A significant increase in bladder volume was recorded eight weeks post-operation due to urinary dysfunction (Fig. 8A). Treatment with the Exo-dECM hydrogel considerably decreased the bladder weight, approaching levels comparable to those in the sham group (Fig. 8B). Morphological assessments, including H&E staining and Masson staining, revealed marked pathological changes, such as thickened bladder walls, intimal hyperplasia, and fibrosis, in the

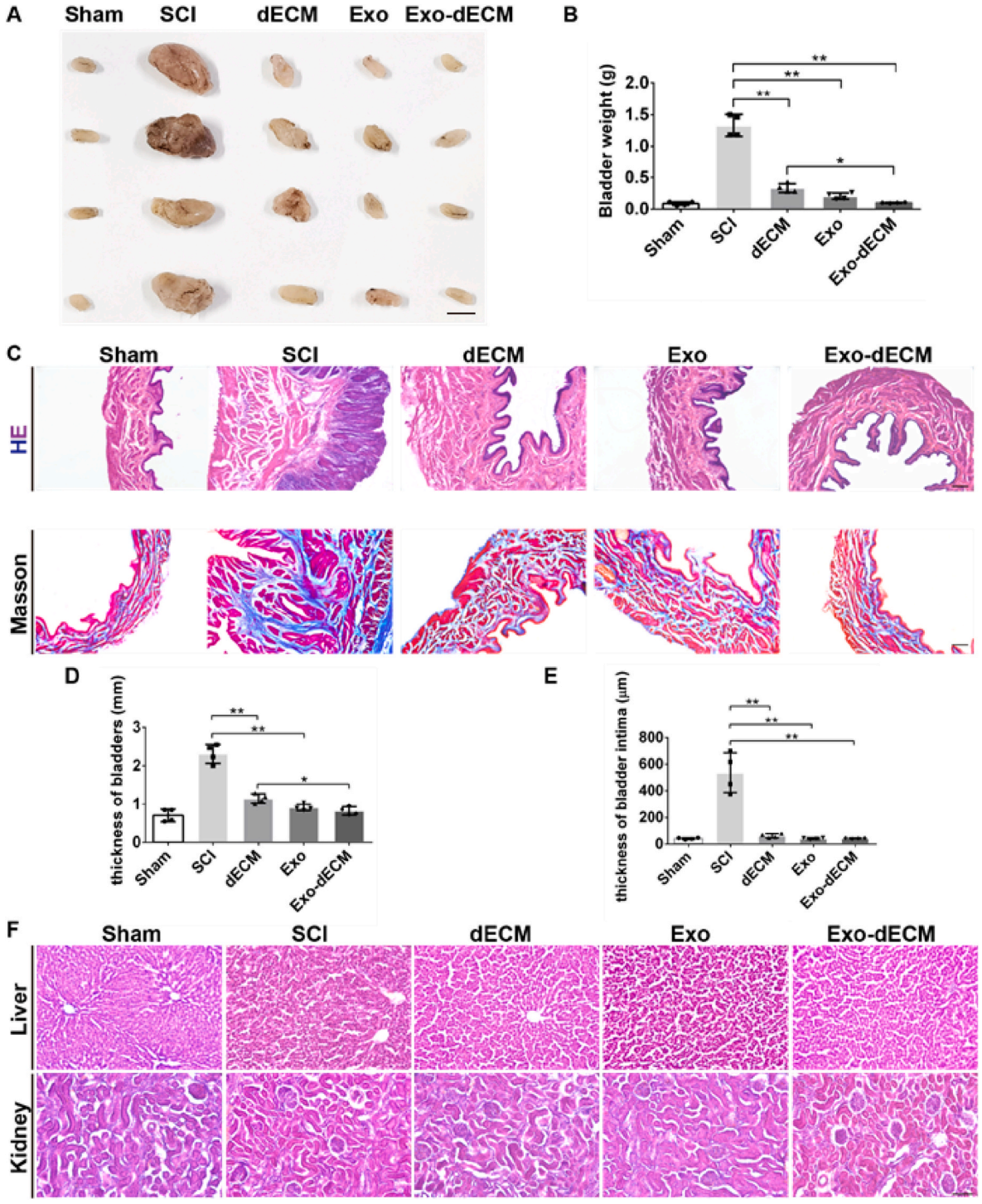

Fig. 8. Examination of bladder tissue. (A) Representative images of bladder tissue at eight weeks after surgery; scale bar: 10 mm. (B) Quantification of the bladder weight at eight weeks after surgery. The graphs show the mean ± SD (n = 4; *$p < 0.05$ and **$p < 0.01$). Each dot represents a rat. (C) Representative images of H&E staining and Masson's trichrome staining of bladder tissues at eight weeks after surgery; scale bar: 200 μm. (D–E) Quantification of bladder thickness and bladder intima thickness. The graphs show the mean ± SD (n = 4; *$p < 0.05$ and **$p < 0.01$). Each dot represents a rat. (F) Representative images of H&E-stained liver and kidney tissues at eight weeks after surgery; scale bar: 100 μm.

bladders of the SCI group (Fig. 8C). Quantitative analyses further demonstrated a substantial decrease in bladder wall and intima thickness following Exo-dECM hydrogel treatment (Fig. 8D and E), indicating the mitigation of pathological damage. These results suggested that Exo-dECM hydrogel intervention can alleviate bladder pathology post-SCI. Additionally, safety assessment through H&E staining of the liver and kidney revealed no apparent pathological changes eight weeks after surgery (Fig. 8F), confirming the safety of treatment.

4. Discussion

Traumatic spinal cord injury (SCI) is a challenging problem due to its limited regenerative capacity, which often leads to significant neurological impairment. Available therapeutic approaches struggle to achieve sustained improvements in motor function post-SCI. One promising avenue involves combining tissue engineering materials with exosomes derived from different cell types in regenerative medicine [32–34]. This study introduced an injectable adhesive Exo-dECM hydrogel comprising a decellularized extracellular matrix and exosomes derived from cortical neurons as a potential therapeutic intervention for SCI. The Exo-dECM hydrogel was found to enhance the local microenvironment, mitigate neuronal apoptosis in the early stages, and promote functional recovery by activating endogenous neural stem cells, facilitating axon regeneration, and supporting remyelination in rats with SCI.

Recent studies have emphasized the significant role of cell-free exosomes, particularly those derived from neuronal cells, in promoting tissue regeneration following SCI [35–37]. However, their clinical application is hindered by their relatively short residence time and insufficient accumulation at the injury site. In this study, we investigated an adhesive dECM hydrogel featuring a complex 3D network structure and favorable cytocompatibility that facilitates the sustained and controlled release of exosomes after *in vivo* administration. Moreover, the dECM hydrogel exhibited notable immunomodulatory and neuroregenerative properties in SCI, potentially enhancing treatment efficacy [17]. The combined action of exosomes and dECM hydrogels may further improve restorative outcomes.

In the initial stages of SCI, CD68-positive inflammatory macrophages are abundant at the injury site. These cells release a range of inflammatory cytokines, such as IL-1β, IL-6, iNOS, IFN-c, TNF-α, interferon-γ, and granulocyte colony-stimulating factor, which contribute to neuronal apoptosis and extensive spinal cord tissue damage [9,10,38]. Several studies have investigated direct immunotherapy as a potential treatment strategy for SCI [39–41]. For example, transplanting M2 microglia into the spinal cord of mice effectively enhanced motor function recovery, improving myelin repair and neuronal survival post-SCI [42]. However, traditional cell transplantation faces challenges, including the need for sourcing cells, ethical concerns, low survival rates, immune rejection, and safety issues. To address these challenges, an alternative approach involving M2 macrophage polarization via bioactive hydrogel transplantation has been investigated. Studies indicate that functional hydrogel transplantation can mitigate inflammation by suppressing macrophage activation and promoting M2 macrophage polarization after SCI [20,43]. Our findings demonstrated a significant increase in M2 macrophages and a modest decrease in M1 macrophages at the lesion site following treatment with the Exo-dECM hydrogel, suggesting a reduction in neuroinflammation and potential mitigation of neuronal apoptosis post-SCI.

Endogenous neural stem cells (NSCs), which are typically quiescent in the spinal cord, become activated in response to SCI [44]. These activated NSCs proliferate, migrate to the injury site, and differentiate into neuronal and neuroglial cells, potentially supporting spinal cord repair [45,46]. *In vivo* studies have shown that activated NSCs predominantly differentiate into astrocytes, contributing to glial scar formation that impedes neural regeneration, with only a small fraction differentiating into neurons [47,48]. Therefore, promoting the differentiation of endogenous NSCs into neurons may facilitate neural regeneration post-SCI. A recent study highlighted that using a cetuximab-modified functional scaffold at the injury site can promote the differentiation of endogenously activated NSCs into neurons, enhancing locomotor recovery following acute complete SCI [49]. Similarly, a modified scaffold transplanted with exogenous NSCs can support the simultaneous differentiation of both endogenous and exogenous NSCs into neurons, aided by the continuous release of neurotrophic molecules at the injury site, thus promoting long-term neuronal differentiation of NSCs for SCI repair [50]. We found a significant increase in Nestin-positive cells in the Exo-dECM hydrogel--treated group, indicating enhanced NSC activation. Furthermore, the presence of NeuN-positive and Tuj1-positive neurons at the lesion site may be attributed to the activation and differentiation of NSCs following Exo-dECM hydrogel treatment. We also noted a slight reduction in glial scar formation with Exo-dECM hydrogel treatment. These findings indicated that Exo-dECM hydrogel treatment promoted endogenous neurogenesis and mitigated glial scar formation to a certain extent, potentially supporting neural repair after SCI.

In our study, the Exo-dECM hydrogel filled the cavity in the spinal cord, providing structural support that promoted axon regeneration and remyelination of the injured tissue. These regenerated nerve fibers, which may be composed of surviving neurons and those derived from activated NSCs, could extend into the lesion site and facilitate the restoration of functionality. Further studies are warranted to differentiate the origin of the extended axons and their specific role in regeneration. Functional assessments revealed significant improvements in hindlimb support, paw grasp, gait, and postural control among the treatment groups, and these improvements were particularly noticeable in the Exo-dECM hydrogel group. SCI disrupts the communication between bladder muscles and the brain, leading to bladder dysfunction [51,52]. The restoration of bladder function serves as an indirect indicator of recovery post-SCI. Morphological and pathological examinations of the bladder, including measurements such as bladder weight, wall thickness, intimal thickness, and fibrosis, supported the observed improvements associated with Exo-dECM hydrogel treatment. Furthermore, impaired conduction function post-SCI can be attributed to physical axonal damage, local hemorrhage, ischemia, demyelination, and the accumulation of chondroitin sulfate proteoglycans [53]. Electrophysiological analyses indicated slightly better motor restoration in the Exo-dECM hydrogel group than in the other groups. The persistence of glial scars and the inability to consistently release exosomes were responsible for the poorer recovery observed in the other comparison groups.

Although the Exo-dECM hydrogel shows promise for SCI treatment, it has several limitations. First, this study exclusively used female rats due to their anatomical suitability and ease of care post-injury. However, it is important to consider potential gender-specific effects influenced by hormone fluctuations such as estrogen levels in cycling female rats, which can affect recovery post-SCI. Future studies should include male rats or both genders to better understand these effects. Second, current dECM hydrogels lack structural organization, and the injectable delivery system used here was designed for single-treatment applications. This highlights the need for developing structured three-dimensional hydrogels and exploring alternative delivery methods in future research. Finally, the molecular mechanisms underlying the therapeutic effects of Exo-dECM hydrogels in improving the microenvironment and promoting tissue repair are only partially understood. Further studies should focus on elucidating these mechanisms, including the synthesis of exosome active ingredients via noncellular pathways *in vitro*. This approach might involve encapsulating these ingredients in sustained-release vesicles integrated into specialized three-dimensional hydrogel structures to enhance the efficacy of SCI treatment.

5. Conclusions

We developed an injectable and adhesive Exo-dECM hydrogel that

incorporates exosomes derived from cortical neurons, demonstrating excellent cytocompatibility and sustained release capabilities to treat SCI. This hydrogel effectively fills post-traumatic cavities and provides mechanical support to injured spinal cord tissue. Our findings indicated that the Exo-dECM hydrogel not only enhances the local microenvironment and reduces early-stage neuronal apoptosis but also stimulates the activation and differentiation of endogenous neural stem cells, while moderately inhibiting glial scar formation. It also synergistically promotes the regeneration of myelinated axons and enhances locomotor recovery. This novel approach of combining cortical neuron-derived exosomes with decellularized extracellular matrix-based hydrogels represents a promising strategy for treating traumatic SCI.

CRediT authorship contribution statement

Gang Wang: Writing – review & editing, Writing – original draft, Software, Formal analysis, Data curation, Conceptualization. **Qian Li:** Visualization, Methodology, Formal analysis. **Sumei Liu:** Visualization, Software, Resources, Methodology. **Mo Li:** Validation, Software, Data curation. **Baoguo Liu:** Software, Investigation, Data curation. **Tianyao Zhao:** Software, Methodology, Formal analysis. **Bochao Liu:** Writing – review & editing, Writing – original draft, Methodology, Investigation. **Zhiguo Chen:** Writing – review & editing, Supervision, Project administration, Methodology, Funding acquisition.

Declaration of competing interest

The authors declare that they have no known competing financial interests or personal relationships that could have appeared to influence the work reported in this paper.

Data availability

The authors are unable or have chosen not to specify which data has been used.

Acknowledgements

This work was supported by grants from Grant sponsors: National Natural Science Foundation of China (82171250), Beijing Municipal Health Commission Fund (PXM2020_026283_000005) and The Project for Techonology Development of Beijing-affiliated Medical Research Institutes (11000023T000002036310).

Appendix B. Supplementary Data

Supplementary data to this article can be found online at https://doi.org/10.1016/j.mtbio.2024.101250IF:%208.7%20Q1.

Appendix A. Supplementary data

Supplementary data to this article can be found online at https://doi.org/10.1016/j.mtbio.2024.101250IF:%208.7%20Q1.

References

[1] C. Li, et al., Role of peripheral immune cells in spinal cord injury, Cell. Mol. Life Sci. 80 (1) (2022).
[2] J. Van Broeckhoven, et al., Macrophage phagocytosis after spinal cord injury: when friends become foes, Brain 144 (10) (2021) 2933–2945.
[3] M.C. Lund, et al., The inflammatory response after moderate contusion spinal cord injury: a time study, Biology 11 (6) (2022).
[4] N. Bahram Sangani, et al., The role of Extracellular Vesicles during CNS development, Prog Neurobiol 205 (2021) 102124.
[5] Y.T.a.Y. Takakura, Extracellular vesicle-based therapeutics: extracellular vesicles as therapeutic targets and agents, Pharmacology & Therapeutics 242 (2023) 108352.
[6] R. Upadhya, et al., Extracellular vesicles from human iPSC-derived neural stem cells: miRNA and protein signatures, and anti-inflammatory and neurogenic properties, J. Extracell. Vesicles 9 (1) (2020) 1809064.
[7] H. Fan, et al., Exosomes derived from olfactory ensheathing cells provided neuroprotection for spinal cord injury by switching the phenotype of macrophages/microglia, Bioeng Transl Med 7 (2) (2022) e10287.
[8] D. Dutta, et al., Extracellular vesicles as an emerging frontier in spinal cord injury pathobiology and therapy, Trends Neurosci. 44 (6) (2021) 492–506.
[9] W.-z. Liu, et al., Mesenchymal stem cell-derived exosomes: therapeutic opportunities and challenges for spinal cord injury, Stem Cell Res. Ther. 12 (1) (2021).
[10] G. Sun, et al., hucMSC derived exosomes promote functional recovery in spinal cord injury mice via attenuating inflammation, Mater. Sci. Eng. C 89 (2018) 194–204.
[11] Q. Chang, et al., Bone marrow mesenchymal stem cell-derived exosomal microRNA-125a promotes M2 macrophage polarization in spinal cord injury by downregulating IRF5, Brain Res. Bull. 170 (2021) 199–210.
[12] L. Fan, et al., Exosomes-loaded electroconductive hydrogel synergistically promotes tissue repair after spinal cord injury via immunoregulation and enhancement of myelinated axon growth, Adv. Sci. 9 (13) (2022).
[13] D. Jiang, et al., Neuron-derived exosomes-transmitted miR-124-3p protect traumatically injured spinal cord by suppressing the activation of neurotoxic microglia and astrocytes, J Nanobiotechnology 18 (1) (2020) 105.
[14] X. Zhang, et al., Exosomes combined with biomaterials in the treatment of spinal cord injury, Front. Bioeng. Biotechnol. 11 (2023).
[15] H. Peng, et al., Research progress of hydrogels as delivery systems and scaffolds in the treatment of secondary spinal cord injury, Front. Bioeng. Biotechnol. 11 (2023).
[16] D. Silva, R.A. Sousa, A.J. Salgado, Hydrogels as delivery systems for spinal cord injury regeneration, Materials Today Bio 9 (2021).
[17] D. Tukmachev, et al., Injectable extracellular matrix hydrogels as scaffolds for spinal cord injury repair, Tissue Eng. 22 (3–4) (2016) 306–317.
[18] Z. Sun, et al., Harnessing developmental dynamics of spinal cord extracellular matrix improves regenerative potential of spinal cord organoids, Cell Stem Cell 31 (5) (2024) 772–787.e11.
[19] J. Ji, et al., Decellularized matrix of adipose-derived mesenchymal stromal cells enhanced retinal progenitor cell proliferation via the Akt/Erk pathway and neuronal differentiation, Cytotherapy 20 (1) (2018) 74–86.
[20] J.Y. Hong, et al., Decellularized brain matrix enhances macrophage polarization and functional improvements in rat spinal cord injury, Acta Biomater. 101 (2020) 357–371.
[21] X. Zhang, et al., Decellularized extracellular matrix and mesenchymal stem cells promote recovery in traumatic brain injury by synergistically enhancing neurogenesis and attenuating neuroinflammation, J. Mater. Sci. Technol. 138 (2023) 17–28.
[22] T.T.A. Liguori, et al., Bioactive decellularized cardiac extracellular matrix-based hydrogel as a sustained-release platform for human adipose tissue-derived stromal cell-secreted factors, Biomedical Materials 16 (2) (2021).
[23] I. Espuny-Camacho, et al., Human pluripotent stem-cell-derived cortical neurons integrate functionally into the lesioned adult murine visual cortex in an area-specific way, Cell Rep. 23 (9) (2018) 2732–2743.
[24] Y. Wei, et al., Pyruvate kinase type M2 promotes tumour cell exosome release via phosphorylating synaptosome-associated protein 23, Nat. Commun. 8 (1) (2017).
[25] L. Wang, et al., MicroRNAs of extracellular vesicles derived from mesenchymal stromal cells alleviate inflammation in dry eye disease by targeting the IRAK1/TAB2/NF-kappaB pathway, Ocul. Surf. 28 (2023) 131–140.
[26] S. Liu, et al., Transplantation of fibrin-thrombin encapsulated human induced neural stem cells promotes functional recovery of spinal cord injury rats through modulation of the microenvironment, Neural Regeneration Research 19 (2) (2024) 440–446.
[27] C. Wang, et al., A bioactive injectable self-healing anti-inflammatory hydrogel with ultralong extracellular vesicles release synergistically enhances motor functional recovery of spinal cord injury, Bioact. Mater. 6 (8) (2021) 2523–2534.
[28] S. Wang, et al., BMSC-derived extracellular matrix better optimizes the microenvironment to support nerve regeneration, Biomaterials 280 (2022) 121251.
[29] Sachin P. Gadani, et al., Dealing with danger in the CNS: the response of the immune system to injury, Neuron 87 (1) (2015) 47–62.
[30] X. Wu, Y. Yan, Q. Zhang, Neuroinflammation and modulation role of natural products after spinal cord injury, J. Inflamm. Res. 14 (2021) 5713–5737.
[31] M. Stenudd, H. Sabelström, J. Frisén, Role of endogenous neural stem cells in spinal cord injury and repair, JAMA Neurol. 72 (2) (2015).
[32] Q. Li, et al., Engineering strategies and optimized delivery of exosomes for theranostic application in nerve tissue, Theranostics 13 (12) (2023) 4266–4286.
[33] J. Huang, et al., Cell-free exosome-laden scaffolds for tissue repair, Nanoscale 13 (19) (2021) 8740–8750.
[34] A. Nagelkerke, et al., Extracellular vesicles for tissue repair and regeneration: evidence, challenges and opportunities, Adv. Drug Deliv. Rev. 175 (2021).
[35] Y. Xu, et al., Neuron-derived exosomes promote the recovery of spinal cord injury by modulating nerve cells in the cellular microenvironment of the lesion area, Mol. Neurobiol. 60 (8) (2023) 4502–4516.
[36] T. Han, et al., Inflammation modifies miR-21 expression within neuronal extracellular vesicles to regulate remyelination following spinal cord injury, Stem Cell Reviews and Reports 19 (6) (2023) 2024–2037.
[37] T. Yu, et al., Exosome-mediated repair of spinal cord injury: a promising therapeutic strategy, Stem Cell Res. Ther. 15 (1) (2024).

[38] H. Tang, et al., The role of immune cells and associated immunological factors in the immune response to spinal cord injury, Front. Immunol. (2023) 13.
[39] R.C. Sterner, R.M. Sterner, Immune response following traumatic spinal cord injury: pathophysiology and therapies, Front. Immunol. 13 (2023).
[40] Y. Feng, et al., The immune microenvironment and tissue engineering strategies for spinal cord regeneration, Front. Cell. Neurosci. 16 (2022) 969002.
[41] A. Al Mamun, et al., Advances in immunotherapy for the treatment of spinal cord injury, Immunobiology 226 (1) (2021).
[42] S. Kobashi, et al., Transplantation of M2-deviated microglia promotes recovery of motor function after spinal cord injury in mice, Mol. Ther. 28 (1) (2020) 254–265.
[43] D.-M. Xie, et al., Modified black phosphorus quantum dots promotes spinal cord injury repair by targeting the AKT signaling pathway, J. Tissue Eng. 14 (2023).
[44] E.A.B. Gilbert, et al., Regulating endogenous neural stem cell activation to promote spinal cord injury repair, Cells 11 (5) (2022).
[45] W. Guo, et al., The roles and applications of neural stem cells in spinal cord injury repair, Front. Bioeng. Biotechnol. 10 (2022).
[46] J. Li, et al., Recent advances in endogenous neural stem/progenitor cell manipulation for spinal cord injury repair, Theranostics 13 (12) (2023) 3966–3987.
[47] C.A. Grégoire, et al., Endogenous neural stem cell responses to stroke and spinal cord injury, Glia 63 (8) (2015) 1469–1482.
[48] Midori A. Arai, a.N.I. a Mitsuha Tanaka, a Kenji Uemura, a Noriko Sugimitsu, a Akiko Suganami, b Yutaka Tamura, b Takashi Koyano, c Thaworn Kowithayakornd, Masami Ishibashi*a, Hes1 inhibitor isolated by target protein oriented natural products isolation (TPO-NAPI) of differentiation activators of neural stem cells†, Chem. Sci. 7 (2) (2016) 1514–1520.
[49] X. Li, et al., Cetuximab modified collagen scaffold directs neurogenesis of injury-activated endogenous neural stem cells for acute spinal cord injury repair, Biomaterials 137 (2017) 73–86.
[50] B. Xu, et al., A dual functional scaffold tethered with EGFR antibody promotes neural stem cell retention and neuronal differentiation for spinal cord injury repair, Adv. Healthcare Mater. 6 (9) (2017).
[51] N.E. Perez, et al., Neurogenic bladder physiology, pathogenesis, and management after spinal cord injury, J. Personalized Med. 12 (6) (2022).
[52] N. Shimizu, et al., Molecular mechanisms of neurogenic lower urinary tract dysfunction after spinal cord injury, Int. J. Mol. Sci. 24 (9) (2023).
[53] N.D. James, et al., Conduction failure following spinal cord injury: functional and anatomical changes from acute to chronic stages, J. Neurosci. 31 (50) (2011) 18543–18555.